Hyporheic exchange with heterogeneous streambeds: Laboratory experiments and modeling

Mashfiqus Salehin,[1] Aaron I. Packman, and Matthew Paradis

Department of Civil and Environmental Engineering, Northwestern University, Evanston, Illinois, USA

Received 7 August 2003; revised 5 May 2004; accepted 25 June 2004; published 4 November 2004.

[1] Hyporheic exchange is generally analyzed with the assumption of a homogeneous hyporheic zone. In reality, streambed sediments have a heterogeneous structure, and this natural heterogeneity produces spatially variable interfacial fluxes and complex hyporheic exchange patterns. To assess the basic effects of sediment structure on hyporheic exchange, we performed salt and dye injection experiments in a recirculating laboratory flume with two heterogeneous sediment beds characterized by negative-exponential correlated random hydraulic conductivity fields. Dye injections showed that the hyporheic flow structure was controlled by the spatial relationship of bed forms to high- and low-permeability regions of the streambed. As no existing model could represent these effects, we developed a new finite element model to calculate the pore water flow field resulting from the interaction of the bed form-induced boundary head distribution and the heterogeneous sediment structure. A numerical particle-tracking approach was then used to assess the resulting hyporheic exchange. The combined flow-transport model did an excellent job of predicting the complex hyporheic flow pathways in the heterogeneous bed and the net hyporheic exchange up to $t \approx 30$ hours. The heterogeneous hydraulic conductivity field caused both greater spatial variability in the water flux through the bed surface and a greater average interfacial flux than would have occurred with a homogeneous bed. The layered correlation structure of the streambed produced an effective anisotropy that favored longitudinal pore water flow and caused a relatively rapid decrease of the mean pore water velocity with depth. As a result, solute penetration into the bed was confined to a more shallow region than would have occurred with a homogeneous bed. The combination of faster near-surface transport and shallower solute penetration produced a shorter mean hyporheic residence time. On the basis of the combination of experimental results and model simulations we conclude that the structural heterogeneity of streambed sediments produces more spatially limited hyporheic exchange that occurs with greater spatial variability and at a higher overall rate. *INDEX TERMS:* 1832 Hydrology: Groundwater transport; 1831 Hydrology: Groundwater quality; 1829 Hydrology: Groundwater hydrology; *KEYWORDS:* heterogeneous streambeds, hyporheic exchange

Citation: Salehin, M., A. I. Packman, and M. Paradis (2004), Hyporheic exchange with heterogeneous streambeds: Laboratory experiments and modeling, *Water Resour. Res.*, *40*, W11504, doi:10.1029/2003WR002567.

1. Introduction

[2] Stream-subsurface exchange is now recognized as a fundamental process that affects the transport and fate of contaminants and other ecologically relevant substances in streams. Aqueous ions can be carried across the stream-subsurface interface into the near-stream subsurface region, called the hyporheic zone, reside there for some time, and then return to the stream. This interfacial transport connects surface waters to sedimentary pore waters, and is thus important for downstream contaminant transport, releases from contaminated sediments, and overall nutrient and carbon dynamics in watersheds [*Brunke and Gonser*, 1997; *Stanford and Gonser*, 1998; *Jones and Mulholland*, 2000; *Medina et al.*, 2004].

[3] A variety of models have been used to analyze hyporheic exchange. The most commonly used model, the Transient Storage Model [*Bencala and Walters*, 1983], idealizes hyporheic exchange in terms of a mean exchange rate with a well-mixed hyporheic zone of constant volume. Other idealized models have considered hyporheic exchange as a diffusive process [e.g., *Cerling et al.*, 1990; *Wörman*, 1998] or as a component of the dispersion induced by dead zones [e.g., *Young and Wallis*, 1993]. Other studies have focused on the representation of the physics of the exchange mechanism at the channel or subchannel scales. Local vertical exchange is generally dominated by advective flows induced by bed forms [*Thibodeaux and Boyle*, 1987; *Savant et al.*, 1987; *Elliott and Brooks*, 1997a, 1997b]. Streamflow over bed forms produces a periodic variation in the dynamic head at the bed surface, which in

[1] Now at Institute of Water and Flood Management, Bangladesh University of Engineering and Technology, Dhaka, Bangladesh.

0043-1397/04/2003WR002567$09.00

turn induces an advective pore water flow into, through and out of the streambed. Pressure-driven advective exchange flows have also been shown to occur in pool-riffle sequences and around other stream features such as meanders, steps, and obstacles [*Harvey and Bencala*, 1993; *Wondzell and Swanson*, 1996; *Wroblicky et al.*, 1998; *Hutchinson and Webster*, 1998]. Similar processes also induce interfacial fluxes through the seafloor [*Huettel et al.*, 1996], and in snowpacks due to wind pumping [*Colbeck*, 1989, 1997]. *Wörman et al.* [2002] have recently developed a model that uses advective pumping theory to analyze solute transport in natural streams. This model has been successfully applied to improve interpretation of the results of recent field tracer experiments [*Salehin et al.*, 2003].

[4] While these recent studies have significantly advanced our understanding of hyporheic exchange processes, no previous studies have explicitly analyzed the effects of streambed structure on hyporheic exchange. *Colbeck* [1997] considered the effect of layered heterogeneity on wind pumping in snowpacks, and found that enhanced flow through high-permeability layers produced shorter flow paths and reduced air penetration. Fluvial sediments normally show much more complicated structure, and this structure is known to play a critical role in the biogeochemistry and ecology of the hyporheic zone [*Boulton et al.*, 1998; *Huggenberger et al.*, 1998; *Baxter and Hauer*, 2000; *Sophocleous*, 2002; *Bradley et al.*, 2002]. Hence there is a clear need to develop both fundamental understanding of the effects of fluvial heterogeneity on hyporheic exchange and practical models for analysis of these effects.

[5] Significant challenges exist in attempting to assess the effects of sedimentary heterogeneity on hyporheic exchange in natural streams. Despite the fact that fluvial morphological processes have been extensively studied, little is known about the fine-scale structure of streambeds. It has long been known that the dynamic processes of aggradation and degradation produce characteristic sediment structure in streambeds [*Leopold et al.*, 1964]. A considerable amount of recent effort has been devoted to improving understanding of the complex relationships between stream flow, sediment transport dynamics, and channel form [e.g., *Robert*, 1993; *Buffington and Montgomery*, 1999a, 1999b; *Lisle et al.*, 2000]. However, practically all of this effort has been devoted to understanding large-scale variations in streambed stratigraphy and channel structure [e.g., *Bridge*, 1993; *Bridge et al.*, 1995; *Vandenberghe and van Overmeeren*, 1999] or trends in grain size distributions that occur because of sediment sorting or selective transport processes [e.g., *Parker and Klingeman*, 1982; *Powell*, 1998; *Church et al.*, 1998; *Whiting and King*, 2003]. While such information is useful for understanding fluvial sedimentary environments and channel formation dynamics at large scales, it provides only limited insight into the fine structure that is responsible for local heterogeneity in hyporheic exchange fluxes. The recent application of ground-penetrating radar to fluvial stratigraphy has made detailed structural information available for some streams [e.g., *Naegeli et al.*, 1996; *Huggenberger et al.*, 1998]. However, there is still no general picture of the local three-dimensional structure of streambed sediments, and in any case there have been no specific investigations of the relationships between fluvial sediment structure, the streambed hydraulic conductivity field, and pore water flows.

[6] On the basis of the above discussion, it should be clear that we lack the requisite information to construct generally representative heterogeneous streambeds for experimental or numerical studies of local hyporheic exchange. To resolve this difficulty in a way that will let us assess the fundamental effects of sediment heterogeneity on hyporheic exchange, herein we employ a geostatistical representation of streambed structure that is based on studies of groundwater flow in alluvial aquifers. Sediment heterogeneity in aquifer formations has been explicitly represented in a number of studies of groundwater flow and transport [e.g., *Bakr et al.*, 1978; *Gelhar and Axness*, 1983; *Neuman et al.*, 1987]. Well-developed methods exist to generate appropriate heterogeneous hydraulic conductivity fields from a user-specified set of statistical parameters [*Ababou et al.*, 1989; *Tompson and Gelhar*, 1990] and to physically construct equivalent heterogeneous sedimentary systems for experimentation [*Welty and Elsner*, 1997; *Chao et al.*, 2000].

[7] The work presented here is the first attempt to explicitly assess the effect of sediment structure on hyporheic exchange. We conducted hyporheic exchange experiments under different flow and sedimentary conditions in a recirculating laboratory flume packed with a heterogeneous sediment bed. We also developed a model for advective hyporheic exchange with detailed and explicit representation of the streambed structure. We generated heterogeneous beds for the experiments and model simulations by employing geostatistical methods developed for studies of alluvial groundwater aquifers with input parameters obtained from our general understanding of fluvial sediment structure. While not necessarily being representative of a particular stream system, this study demonstrates the basic effects of subsurface heterogeneity on stream-subsurface flow coupling and the resulting hyporheic exchange. The combination of experimental results and numerical simulations provides valuable insight into the effects of streambed heterogeneity on interfacial water fluxes, pore water flows, solute penetration into the subsurface, and the residence time of stream-derived solutes in the hyporheic zone.

2. Analysis of Advective Hyporheic Exchange With a Heterogeneous Streambed

[8] Several steps are required to analyze advective hyporheic exchange with a heterogeneous streambed. First, the governing equations for the pore water velocity field are derived from basic principles. These equations can be solved analytically when the bed is homogeneous, but a numerical solution is required when the bed is heterogeneous. A finite element model is employed here in order to explicitly represent the sediment structure. The finite element model calculates the subsurface head distribution and pore water velocity field, from which the local and average water flux across the stream-subsurface interface are directly obtained. The resulting solute exchange is determined by the residence time approach, with a particle-tracking model used to calculate the subsurface residence time distribution from the pore water velocity field. The net change in the in-stream solute concentration is related to the interfacial flux

and subsurface residence time distribution by a convolution integral.

2.1. Pore Water Velocity Field: Governing Equations

[9] The interstitial velocity field based can be found by the solving the two governing equations, Darcy's law (1), and the equation of continuity (2):

$$\bar{v} = -K\nabla h \tag{1}$$

$$\nabla.\bar{v} = 0 \tag{2}$$

where K is the hydraulic conductivity, $\bar{v}$ = (u, v) is the Darcy pore water velocity vector, and h is the hydraulic head. For a homogeneous bed, the hydraulic conductivity, K, is a constant, and the governing equations (1) and (2) yield Laplace's equation, which can readily be solved for given boundary conditions expressed in terms of head or velocity. *Elliott and Brooks* [1997a] found that the head distribution over dune-shaped bed forms could be approximated well by a sinusoidal profile:

$$h = h_m \sin(kx) \tag{3}$$

$$h_m = 0.28\frac{V^2}{2g}\begin{cases}\left(\dfrac{H/d}{0.34}\right)^{3/8} & H/d \le 0.34\\ \left(\dfrac{H/d}{0.34}\right)^{3/2} & H/d \ge 0.34\end{cases} \tag{4}$$

where k is the bed form wave number ($k = 2\pi/\lambda$; λ is the dune wavelength), x is the longitudinal coordinate along the streambed, h_m is the half amplitude of the head variation, V is the mean stream velocity, H is the dune height (trough to crest), d is the mean stream depth, and g is the acceleration due to gravity. Note that the coordinate system used here has the coordinate x parallel to the mean streambed surface, and the orthogonal coordinate y perpendicular to the bed surface. This coordinate system varies slightly from the horizontal because of the small slope of the stream in uniform flow. Using the surface pressure distribution equations (3) and (4) as a boundary condition, an analytical solution of the pore water velocity field was obtained by *Elliott and Brooks* [1997a] for an infinite homogeneous bed and by *Packman et al.* [2000a] for a finite homogeneous bed.

[10] For a heterogeneous sediment bed, the hydraulic conductivity is variable in space. In this case, the governing equations (1) and (2) yield the following equation for a two-dimensional, steady state flow system:

$$\frac{\partial}{\partial x}\left(K_{xx}\frac{\partial h}{\partial x}\right) + \frac{\partial}{\partial y}\left(K_{yy}\frac{\partial h}{\partial y}\right) = 0 \tag{5}$$

where K_{xx} and K_{yy} are the hydraulic conductivities in the principal x and y directions.

2.2. Pore Water Velocity Field: Numerical Model

[11] A two-dimensional Galerkin weighted-residual type finite element model (FEM) was developed using triangular elements to solve equation (5) for the pore water head field. This model has the capability to represent arbitrary bed geometries, boundary conditions, and any sediment structure including a homogeneous-isotropic medium (in which case equation (5) reduces to Laplace's equation), a heterogeneous-isotropic medium ($K_{xx} = K_{yy}$), or a heterogeneous-anisotropic medium ($K_{xx} \neq K_{yy}$). Pore water heads (h) are calculated at each node and the head gradients ($\partial h/\partial x$ etc.) are calculated in each element. The interstitial velocity is calculated as the Darcy velocity, $u = K_{xx}$ ($\partial h/\partial x$) and $v = K_{yy}$ ($\partial h/\partial y$).

[12] The model was employed here with the sinusoidal pressure distribution given in equations (3) and (4) as the upper boundary condition, a no flow boundary condition at the bottom of the sediment bed (considered impermeable), and a periodic boundary condition at the upstream and downstream boundaries. The periodic boundary condition was implemented by overwriting the element stiffness matrix equations with $h_i = h_j$, where 'i' and 'j' are the matching nodes at the upstream and downstream boundaries. The sediment structure was explicitly represented as described in section 3.

2.3. Hyporheic Exchange Mass Transfer: Theory

[13] The mass transfer to the streambed (hyporheic exchange) is calculated using the residence time function approach, following *Elliott and Brooks* [1997a]. The residence time function, $R(\tau, x)$, is the probability that tracer that enters the bed at position x will remain in the bed after an elapsed time τ. Net mass transfer depends on the average residence time function for exchange through the entire streambed, $\bar{R}(\tau)$, which is:

$$\bar{R}(\tau) = \frac{\dfrac{1}{L}\displaystyle\int_{x=0}^{x=L} q(x)R(\tau, x)dx}{\bar{q}} \tag{6}$$

where q(x) is the local water flux into the bed and L is the total length of the bed surface and $\bar{q}$ is the average flux over the entire bed surface. The interfacial water flux, q, is calculated directly from the pore water velocity field:

$$q(x) = \begin{cases}\bar{v}\cdot\bar{n} & \text{if } \bar{v}\cdot\bar{n} \ge 0\\ 0 & \text{if } \bar{v}\cdot\bar{n} < 0\end{cases} \tag{7}$$

where $\bar{n}$ is the unit vector normal to the bed surface pointing outward. The average flux, $\bar{q}$, is found by taking the average of the absolute value of $\bar{v}\cdot\bar{n}$ over the entire bed surface (0 to L). Note that this is equivalent to taking the average of equation (7) over the area of positive flux. The residence time function $\bar{R}(\tau)$ has a value of 1 at $\tau = 0$ and decreases over time as solute leaves the bed. For a conservative solute, $\bar{R} \to 0$ as $\tau \to \infty$ since there is no permanent retention of conservative solutes in the streambed.

[14] In general terms, net mass transfer between the stream and subsurface can be determined from the interfacial water flux, the solute concentration history in the stream, and the subsurface residence time distribution. *Wörman et al.* [2002] and *Haggerty et al.* [2002] have shown how subsurface residence time distribution functions can be used to analyze hyporheic exchange in natural

streams. Here, to analyze the results of laboratory experiments in a closed recirculating flume, we only need to consider a simple mass balance between the stream and subsurface. Further, we conducted experiments with the initial condition that that solute concentration has a value of C_0 everywhere in the stream, and a value of zero everywhere in the bed. In this case, mass transfer to the streambed is conveniently represented by the average depth of solute penetration into the subsurface, M. For these conditions, mass balance between the stream and subsurface gives:

$$C^*(t) = \frac{d'}{d' + M(t)\theta} \tag{8}$$

where $C^*(t) = C(t)/C_0$ is the normalized in-stream solute concentration at time t, C(t) is the in-stream solute concentration at time t, d' is the effective depth (the total volume of recirculating water in the flume per unit bed surface area), and θ is the porosity of the sediment bed. The change in the in-stream concentration is also related to the solute flux across the stream-subsurface interface by:

$$M(t)C(t) = \frac{\bar{q}}{\theta}\int_0^t \bar{R}(\tau)C^*(t-\tau)d\tau \tag{9}$$

Net hyporheic exchange is determined by simultaneous solution of equations (8) and (9), and can be represented equivalently by either M(t), C(t), or C*(t). Further information on the residence time function approach is given by *Elliott and Brooks* [1997a].

2.4. Hyporheic Exchange Mass Transfer: Numerical Model

[15] A numerical model was developed to analyze the net mass transfer of solutes into heterogeneous streambeds. The model has three principal components: (1) the finite element model described in section 2.2 was used to calculate the pore water flow field and interfacial water flux for given streamflow conditions and sediment structure, (2) a numerical particle tracking model was used to calculate the resulting hyporheic residence time distribution, and (3) equations (8) and (9) were solved simultaneously by numerical integration.

[16] The particle-tracking model is implemented in a finite difference form to directly calculate the flux-weighted average residence time function, $\bar{R}(\tau)$, from the pore water velocity field. Solute transport is represented by a large number of virtual particles, typically 2000 per bed form, that are initially evenly spaced over the bed surface. Each particle is assigned a weight equivalent to the local interfacial water flux as given by equation (7). Starting at t = 0, the particles are displaced in the pore water according to the local Darcy velocity in small time-increments, typically 10s in the simulations reported here. In each time step, the local velocity must be found from the results of the finite element model. An efficient search routine is used to relate the particle positions to the nearest node numbers and neighboring elements in the finite element model. With this information, the positions of all particles are tracked as they propagate through the bed. The average residence time distribution, $\bar{R}(\tau)$, is calculated at each time step as the ratio of the total weight of the particles still in the bed to the initial total weight. The calculation is repeated until all particles leave the bed.

[17] After the residence time distribution is found, it is used along with the interfacial flux to calculate hyporheic exchange according to equation (9). The change in the in-stream concentration is tracked over time and related to the solute penetration into the subsurface by equation (8). The convolution integral (9) is numerically integrated in a straightforward fashion.

[18] Application of this approach to the analysis of hyporheic exchange with a heterogeneous bed requires considerably more computational resources than needed to analyze exchange with a homogenous bed. For a homogeneous bed, the sediment structure is the same underneath each bed form. In addition, the interfacial flux generally scales simply with the bed form size. In this case, hyporheic exchange can be directly averaged over the entire streambed, and model simulation of exchange with a single bed form of average size can be used to represent the net exchange with the entire bed [*Elliott and Brooks*, 1997a, 1997b; *Packman et al.*, 2000a, 2000b]. For a heterogeneous sediment bed, the flux through each bed form depends on the local sediment structure, and thus the computation of exchange must be carried out over the entire streambed. This requires that the entire experimental domain be represented in the numerical model, with the complete bed geometry and sediment structure represented explicitly.

3. Representation of Heterogeneous Streambeds

[19] In order to assess the effects of sediment heterogeneity on hyporheic exchange, we had to generate an appropriate streambed structure that could be constructed in a laboratory flume. A random field generator was used to design correlated random hydraulic conductivity fields that represent the heterogeneous streambeds. Input parameters used to generate the hydraulic conductivity fields were selected based on guidance from previous studies of the heterogeneity of alluvial aquifers and knowledge of the structure of stream channels.

3.1. Geostatistical Description of Sediment Structure

[20] Subsurface hydraulic conductivity, K, is generally not purely random but displays an underlying correlation structure [*Journel and Huijbregts*, 1978]. Numerous examples in the literature suggest that K can be represented as a lognormally correlated random field in space. The degree of heterogeneity is normally expressed as the variance, $\sigma^2_{\ln K}$, and the structure is described by the spatial covariance of lnK in each direction. Generally, lnK is assumed to be a second-order stationary variable, i.e., its mean is constant and the covariance depends only on the separation distance, s, and not on the location. In this case, a covariance analysis is carried out where the variogram, $\gamma(s)$, is related to covariance by:

$$\gamma(s) = [\mathrm{Cov}(s=0) - \mathrm{Cov}(s)] = \sigma^2_{\ln K} - \mathrm{Cov}(s) \tag{10}$$

For a discrete set of measured K data, an experimental variogram is calculated as the mean squared differences

between sample values at specified separation distances. For N(s) number of data pairs, this is:

$$\gamma(s) = \frac{1}{2N(s)} \sum_{i=1}^{N(s)} [\ln K(X_i + s) - \ln K(X_i)]^2 \quad (11)$$

In many studies, a negative exponential model has been found to adequately represent the observed discontinuous experimental variograms:

$$\gamma(s) = \sigma^2_{\ln K}\left(1 - e^{-s/l}\right) \quad (12)$$

where l is the correlation scale, the characteristic distance over which the hydraulic conductivity field is correlated. The correlation length scale can have a different value in different directions.

[21] The turning bands method of *Tompson et al.* [1989] was used to design two-dimensional heterogeneous sediment beds. This method generates a single realization of a second-order stationary, lognormally correlated, multidimensional random permeability field with user specified correlation scales (here l_x and l_y), mean permeability ($\overline{\ln K}$), and variance ($\sigma^2_{\ln K}$) such that the generated lnK field follows the negative exponential model. To be able to be constructed in an experimental system, the variogram must be represented in terms of a number of discrete permeabilities corresponding to distinct sediment size classes. Further, the variogram must also be sampled in terms of blocks of specified geometry that can be used to construct the experimental sediment bed. The sand-substitution procedure developed by *Welty and Elsner* [1997] was used to generate the experimental bed structures based on the permeability field generated by the turning bands code. Statistical parameters, sediments, and methods used to construct the experimental bed are described below.

3.2. Selection of Streambed Design Parameters

[22] There are several issues associated with the design of heterogeneous sediment beds for laboratory experiments involving hyporheic exchange. The key issue is to select appropriate statistical parameters to generate a realistic streambed permeability structure. To generate the heterogeneous beds by the turning bands method, we had to specify the mean and variance of the lognormal hydraulic conductivity field, and the correlation length scales in the horizontal and vertical directions. Our objective was to select these parameters to provide a reasonable representation of a streambed, with the constraint that the resulting bed had to be able to be constructed in a small recirculating flume.

[23] A wide variety of sediments can be found in streams. Here we focus on sandy streambeds and select a mean permeability of 1.8×10^{-6} cm^2, which can be found in sand or sand-and-gravel streambeds. This particular value of mean permeability was selected to match the permeability of Ottawa F-12 Flint silica sand, a well-rounded and well-sorted river sand with a geometric mean diameter of 480 μm that we have extensively used in previous studies of hyporheic exchange [*Packman et al.*, 2000b; *Ren and Packman*, 2002]. Choice of this value allows us to directly compare the results of experiments with homogeneous and heterogeneous beds having the same mean permeability.

[24] There are numerous field data on the permeability structure of groundwater aquifers [*Hess et al.*, 1992; *Rehfeldt et al.*, 1992], but as far as we are aware there are no such data available for active stream channels. Because of the lack of information on the permeability structure of different stream types, we must depend on a more general geostatistical description of alluvial sediment structure to advance our understanding of the role of heterogeneity in hyporheic exchange. *Gelhar* [1993] summarized values of $\sigma^2_{\ln K}$ from a large number of groundwater systems and found $0.25 < \sigma^2_{\ln K} < 4.6$ for glacial outwash sand and gravel aquifers. As these types of aquifers were deposited by fluvial/alluvial processes, they can be expected to have a similar structure to streambeds. Because we wanted to clearly demonstrate the effects of heterogeneity on hyporheic exchange, we selected design values corresponding to a moderately high degree of heterogeneity, $\sigma^2_{\ln K} = 1.0$, and a high degree of heterogeneity, $\sigma^2_{\ln K} = 2.0$. These will be referred to here as the lower heterogeneity case and the higher heterogeneity case, respectively.

[25] *Gelhar* [1993] also reported that subsurface formations typically exhibit an overall anisotropy, with the ratio of the horizontal and vertical correlation scales found to vary from 2:1 to 10:1. We selected a ratio of 10:1, on the high end of what is typically found in groundwater aquifers, because streambed sediments are known to show a strong horizontal layered structure, which arises from the dominant sediment transport in the downstream direction. The specific design values of the correlation length scales were limited both by the size of the experimental system and the need to be able to physically construct the heterogeneous bed. It is preferable for the scale of the experiment to be large enough to satisfy the ergodicity requirements of the stochastic theory. In order for the ergodicity assumption to hold, the domain length should be on the order of 10–100 times the correlation scale of the hydraulic conductivity field in each direction. If this condition is met, the statistical parameters (mean and variance) of one realization of the random field are equivalent to those that would be obtained by averaging over many realizations of the random field. We selected correlation length scales of $l_x = 10$ cm and $l_y = 1$ cm, which reasonably meet the ergodicity requirements in each direction while not presenting undue difficulties in constructing the bed. The sediment bed used for this work had a length of 210 cm, which provides 21 correlation scales in the longitudinal direction. Two bed depths were used, providing 13 and 20 correlation length scales in the normal direction, respectively.

[26] In evaluating the appropriateness of the selected bed parameters, it is important to consider how the geostatistical theory is employed here. We used the negative exponential correlated random field model to generate representative heterogeneous beds with effective anisotropy ($l_x > l_y$) in a reproducible and statistically well-defined fashion. From this, we obtained two particular realizations of heterogeneous beds, as described below, and we used these two realizations by first physically constructing them for experiments and then explicitly representing their structure in our finite element model for calculation of the pore water flow fields. The insight we gain from these experiments and numerical simulations on the role of streambed heterogeneity in hyporheic exchange is expected to be relevant to natural streams. While different types of streams and rivers are expected to

Table 1. Properties of Sands Used to Construct Heterogeneous Streambeds[a]

Sand Class	Permeability, cm^2	s_k,[b] cm^2	θ	d_{50}, mm	d_{10}, mm
4	4.37E-05	±0.23E-05	0.42	3.40	2.40
3	2.00E-05	±0.04E-05	0.43	2.25	1.78
0	4.47E-06	±0.08E-06	0.44	0.80	0.60
F12	1.82E-06	-	0.38	0.50	0.20
00	1.11E-06	±0.04E-06	0.43	0.47	0.15
000	4.51E-07	±0.22E-07	0.44	0.15	0.10
−50	2.07E-07	±0.64E-07	0.42	0.12	0.10

[a]Read 4.37E-05 as 4.37×10^{-5}.
[b]Note that standard deviation of permeability measurements, s_k, were based on 27 measurements for each sand class.

have different underlying sedimentary structure, depending for example on the recent history of sediment supply, watershed hydrology, and other related factors, we still expect that sediment heterogeneity will have a fundamentally similar influence on hyporheic exchange in all cases.

3.3. Generation of Heterogeneous Hydraulic Conductivity Fields

[27] The turning bands code of *Tompson et al.* [1989] was used to generate two sets of two-dimensional correlated random permeability fields having dimensions of 210 cm × 20 cm for the lower heterogeneity case and 210 cm × 13 cm for the higher heterogeneity case. In order to obtain better resolution of the horizontal variogram at small separation distances, we chose to design the bed with 5 cm long × 1 cm thick sand blocks. This provides at least two measurement points within one horizontal correlation scale (10 cm). We would have preferred to also make the vertical block dimension half of the vertical correlation length scale (or less), but we thought it would be practically infeasible to construct the bed in half-centimeter layers. With the 5 cm × 1 cm block size, there were 1020 and 840 discrete blocks for the higher and lower heterogeneity cases, respectively.

[28] We represented the correlated random fields generated by the turning bands code with discrete permeabilities corresponding to the silica sands listed in Table 1. The F12 sand was obtained from U.S. Silica (Ottawa, Illinois), and the remaining sands were obtained from Ricci Brothers and Sons (New Jersey). The hydraulic conductivity of the F12 sand was known from previous studies, and the hydraulic conductivities of the Ricci Brothers sands were measured using a constant head permeameter. The continuous permeability fields generated by the turning bands code were replaced with the discrete sand permeabilities on a block-by-block basis. The complete range of permeability values in each bed design was subdivided into classes, with class cutoffs corresponding to the geometric means of the adjacent sand permeability values. Each sediment block was then assigned the appropriate sand permeability value. This procedure yielded well-defined heterogeneous permeability fields that could be constructed using the available sands. All seven sands listed in Table 1 were required to adequately represent the higher heterogeneity case, but only six were required to represent the lower heterogeneity case (with the −50 sand omitted). The resulting two-dimensional heterogeneous bed designs are shown in Figure 1. The horizontal and vertical variograms for these beds follow the negative exponential model, as shown in Figure 2. The methods used to construct sediment beds matching these designs are described in the next section.

4. Experimental Methods

[29] We conducted a series of experiments to observe hyporheic exchange with a heterogeneous bed in a small recirculating laboratory flume. These experiments allowed ready examination of pore water flow patterns and net hyporheic exchange under controlled flow conditions. The particular flume used in this study has a test section of 210 cm, a channel width of 20 cm, and a depth of 1 m. The channel walls are transparent, which allowed direct measurement of the bed geometry and observation of dye transport in pore waters. The flume features a computer-controlled variable speed pump and a vortex shedding flowmeter (Rosemont model 8800) built into the return circuit. Although the flume is relatively small for open channel flow studies, previous hyporheic exchange experiments in similar small flumes yielded results that agree with measurements made in much larger flumes.

4.1. Construction of Heterogeneous Sediment Bed in the Recirculating Flume

[30] A divider system was designed and fabricated to allow emplacement of the heterogeneous beds in the flume. This

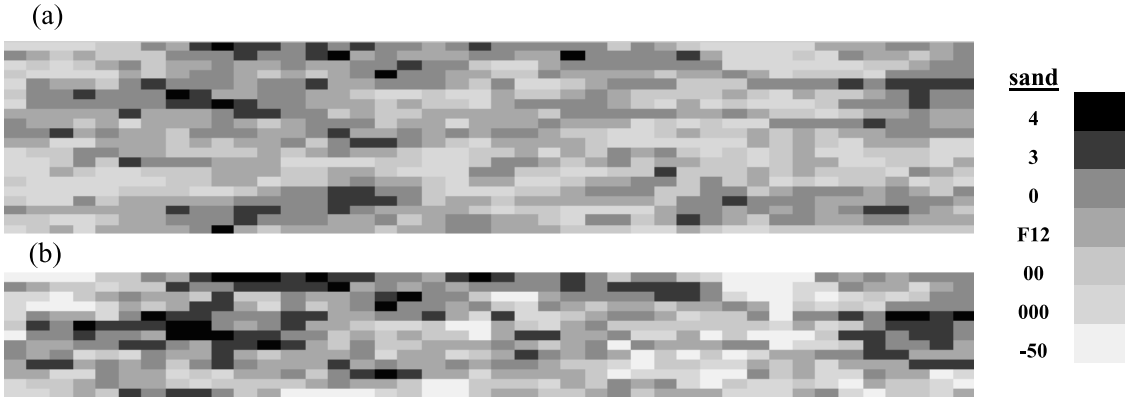

Figure 1. Two-dimensional heterogeneous packing designs based on synthetic generation of correlated random hydraulic conductivity fields: (a) Lower heterogeneity case and (b) higher heterogeneity case. Each block is 5 cm × 1 cm. See color version of this figure at back of this issue.

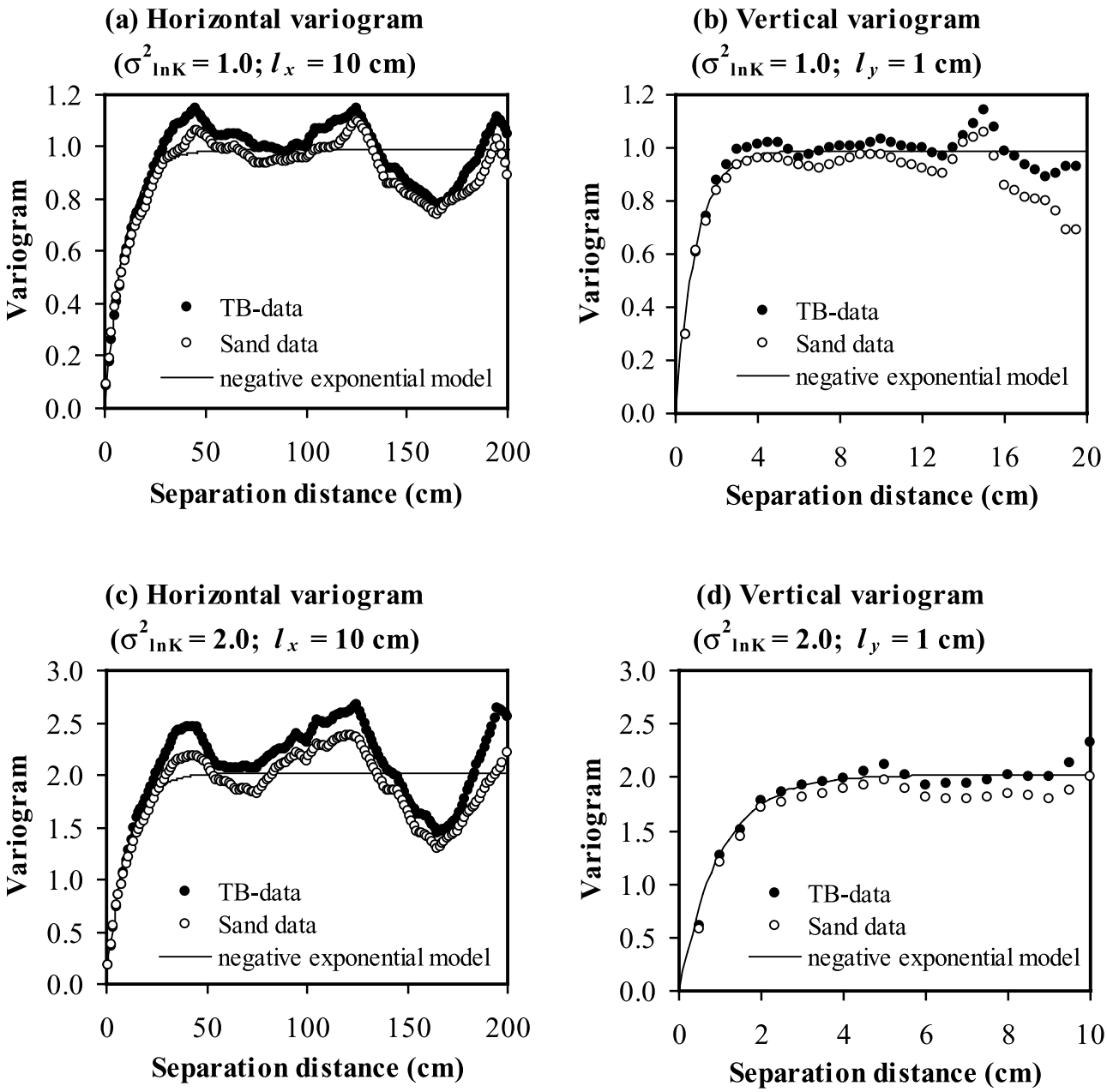

Figure 2. Variograms of lnK for low- and high-variance sediment bed designs. Note differences in x axis scales for horizontal and vertical variograms and in y axis scales for high- and low-variance designs.

system consists of 41 dividers made of 20 cm × 10 cm × 1/8 cm PVC sheets, which were mounted vertically on two long steel rods that were aligned along the axis of the flume. For this work, the dividers were spaced 5 cm apart to match the statistical block design. This apparatus was connected to a winch so it could be raised or lowered uniformly inside the flume.

[31] The flume was packed wet by partially filling the channel with water and then adding sands to form the heterogeneous block pattern. All sands were prewashed before use to remove fines. The volume of sand necessary for each block was premeasured and placed in color-coded plastic cups. To facilitate precise placement of each sand block, a grid of 5 cm × 1 cm cells was drawn on the transparent sidewall of the flume, and each cell was color-coded according to the sand type that should be placed in it. The divider system was lowered to the bottom of the channel and each 5 cm × 1 cm cell was filled with the appropriate sand using a funnel connected to a tube held just above the water surface. Each sand block was made level at 1 cm thick by tapping with a small, perforated horizontal plastic plate. After each three layers of sand were placed, the divider was raised by approximately 2 cm to allow the freshly packed sediments to consolidate into the space previously occupied by the dividers. This caused a small amount of blending of the sand blocks at the edges, but this did not appear to significantly influence the experimental results. Figure 3 shows the bed with the lower heterogeneity in the flume.

Figure 3. Lower heterogeneity bed in the recirculating flume. The grid on the channel sidewall is color-coded to indicate the sand type in each block. See color version of this figure at back of this issue.

[32] Once the heterogeneous bed was in place, a uniform layer of Ottawa F12 sand approximately 2.5 cm thick was placed over the bed surface, and triangular bed forms were manually formed in this homogeneous sediment layer. This approach was used to produce regular dune-shaped bed forms and to ensure that finer sediments were not mobilized under the flow conditions used in the solute injections. We considered the possibility of extending the heterogeneous bed to include bed forms, but it would have been logistically extremely difficult to produce heterogeneous bed forms of a realistic shape. We deemed it preferable to form homogeneous bed forms from the F12 sand, which has the same permeability as the mean of the underlying heterogeneous bed. The presence of a thin layer of F12 sand at the top of the bed thus does not alter the mean bed permeability, and it also does not significantly alter pore water flow patterns.

[33] Two different bed depths were used. The average bed depth was 22.5 cm for the lower heterogeneity case and 15.5 cm for the higher heterogeneity case. These depths include both the lower, heterogeneous portion of the bed and the overlying homogeneous F12 sand layer with bed forms. The lower heterogeneity bed was constructed and tested first. As the initial results suggested that hyporheic exchange was not influenced by the lower part of the bed, and the introduced solute did not penetrate to the bottom of the bed during the course of the experiments, the higher heterogeneity bed was subsequently constructed with a smaller depth. Packing the sediments into the flume required a considerable effort, so use of a shallower bed minimized the effort required to construct the second heterogeneous bed. It took us approximately three weeks to construct the lower heterogeneity bed, and approximately two weeks to construct the higher heterogeneity bed.

4.2. Salt Injection Experiments

[34] A series of salt injection experiments was executed with the flow and sedimentary conditions listed in Table 2. The streamflow velocity and bed topography were varied in order to evaluate hydrodynamic and geomorphic controls on solute exchange with a heterogeneous bed. In different experiments, the mean stream velocity was varied between 10 and 17 cm/s. The stream Reynolds number was greater than 10^4 in all cases. Solute injections were performed with two bed form wavelengths, λ = 15 cm and 25 cm, for each heterogeneous bed. When the longer-wavelength bed forms were used, there were 8 bed forms present on the streambed. There were 13 bed forms when the smaller wavelength was used.

[35] A sodium chloride (NaCl) solution prepared from reagent-grade salt was used as a conservative tracer. The tracer was added uniformly to the recirculating stream in the flume over one recirculation period, and the decrease in the tracer concentration due to exchange with sedimentary pore water was monitored over time. As described in the theory section, this experimental approach is equivalent to the initial condition where there is a uniform in-stream concentration C_0 and no solute in the streambed at t = 0. Thus the decrease in the in-stream concentration is directly related to the mass transfer to the bed. The initial in-stream NaCl concentration was typically 300 mg/L above the preexisting background salt concentration in each experiment. Salt concentrations were measured using a Horiba ES-12 conductivity meter. The net tracer exchange with the bed was calculated from the rate of change of solute concentration in the stream by considering the mass balance between the recirculating stream and pore water in the sediment bed, given by equation (8).

4.3. Dye Injection Experiments

[36] In order to visualize solute transport in the heterogeneous sediment bed, two dye injections were made with

Table 2. Conditions for Flume Tracer Experiments

Experiment	Tracer	σ^2_{lnK}	d_b, cm	λ, cm	H, cm	d, cm	V, cm/s
1	salt	1.0	22.5	15.0	3.0	14.5	15.0
2	salt	1.0	22.5	25.0	3.0	14.5	17.0
3	salt	2.0	15.5	25.0	2.0	14.5	16.5
4	salt	2.0	15.5	25.0	3.0	14.5	10.1
5	salt	2.0	15.5	15.0	2.0	14.5	10.2
6	salt	2.0	15.5	25.0	3.0	14.5	14.0
7	dye	2.0	15.5	25.0	3.0	14.5	14.0
8	dye	2.0	15.5	25.0	3.0	14.5	10.1

Sensient FD&C Blue No.1 and FD&C Red No. 40. These dye injections are designated experiments 7 and 8, respectively. The dyes were stable and did not sorb to sediments. Dye injection experiments were conducted exactly in the same manner as salt tracer experiments, except that the main data were observations of dye penetration into the subsurface. A dye solution was prepared to a desired color from dry powder, and these solutions were injected into the stream over one recirculation period. Dye was readily observed to propagate into the streambed. Dye penetration was photographed at various times, and dye front locations were traced on the transparent sidewall of the flume. Following each experiment, the recorded dye fronts were traced onto transparent sheets and digitized. The average depth of solute penetration, M(t), was determined directly from the digitized dye penetration data. As bed form-induced hyporheic exchange is dominated by advection, the dye fronts were sharp enough that the error in tracing the front positions was only on the order of a few grain diameters, i.e., 1–2 mm. Note that many previous studies have established that pore-scale dispersion is insignificant relative to advection for the case of bed form-induced hyporheic exchange (see particularly *Elliott and Brooks* [1997a, 1997b] for a discussion of this issue).

5. Model Application

[37] The numerical models described in Section 2 were applied to analyze the experimental results. In addition to applying the finite element model to explicitly represent the bed sediment structure, we also simulated hyporheic exchange with a homogeneous bed of the same mean permeability. FEM simulations of exchange with a homogeneous bed were found to give the same results as the analytical model for this case (results not shown).

[38] To model exchange with the heterogeneous bed, the numerical domain had to include the entire sediment bed. The finite element grids for the pore water flow model required between 5500–8000 nodes and 6000–9000 elements for the lower heterogeneity case, and 3500–5500 nodes and 5000–7000 elements for the higher heterogeneity case. Numerical calculation of the pore water flow field required between 1 and 2 hours of CPU time on a Pentium Xeon dual-processor workstation with a clock speed of 933 MHz. Calculation of the residence time function was carried out using 2,000 virtual particles per bed form. This yielded a total of 16,000 virtual particles for simulation of experiments with bed forms of λ = 25 cm, and 26,000 virtual particles for experiments with λ = 15 cm. The particle tracking calculation required 4–5 hours of CPU time, and the numerical integration of equations (8) and (9) required an additional hour. Overall, simulation of hyporheic exchange with the heterogeneous beds increased the computational time by two orders of magnitude relative to analysis of exchange with homogeneous beds.

6. Results

[39] Eight flume experiments were performed, with experiments 1–6 being salt injections and experiments 7–8 being dye injections. The results of salt injection experiments are presented in Figures 4–6 as the change in the normalized in-stream solute concentration over time, $C^*(t) = C(t)/C_0$. Figure 4 compares experimental results with simulations of hyporheic exchange with a homogeneous sediment bed, while Figure 5 displays the results of numerical simulations with explicit representation of the complete heterogeneous bed structure. In both cases, the model simulations are true predictions based on measured inputs, and the models were not fit to the data in any way.

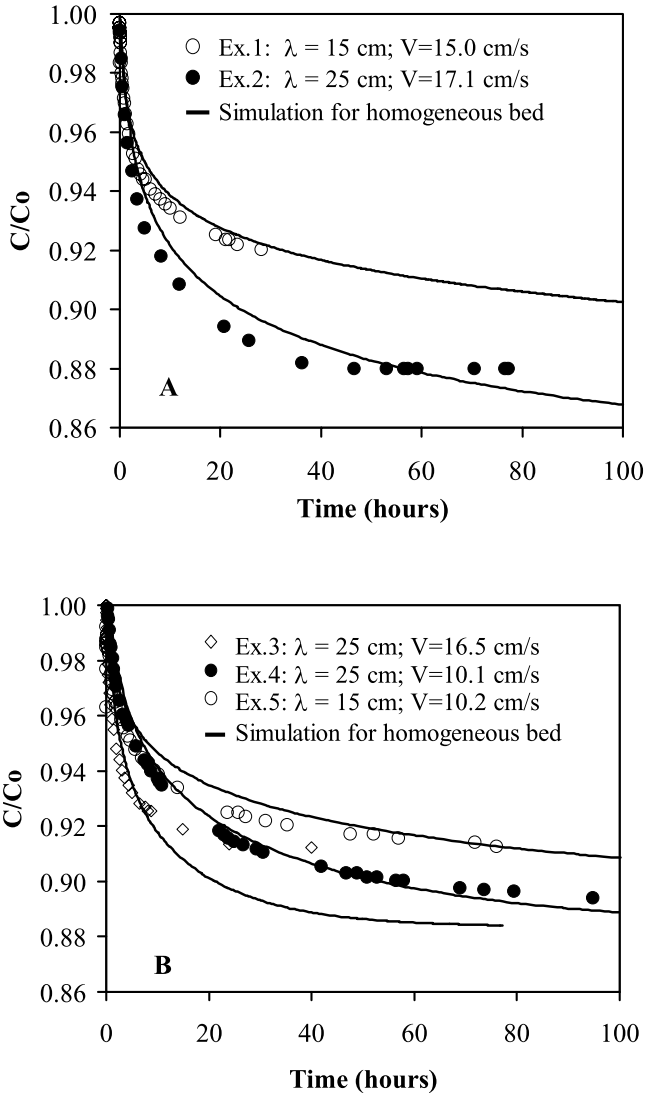

Figure 4. Comparisons of salt exchange results for heterogeneous beds and model simulations for homogeneous beds with the same mean permeability: (a) Lower heterogeneity case (d_b = 22.5 cm) and (b) higher heterogeneity case (d_b = 15.5 cm).

[40] As found in previous studies [e.g., *Elliott and Brooks*, 1997b; *Packman et al.*, 2000b], the stream velocity was observed to have a major effect on stream-subsurface exchange. The higher velocity in experiment 3 caused faster exchange than that in experiment 4, even though all other experimental conditions were the same. In general, the rate of exchange is expected to vary with V^2, because advective pumping exchange is induced by the variations in the dynamic head distribution over bed forms [*Packman and Salehin*, 2003]. The effect of bed form wavelength on exchange can be seen by comparing experiments 4 and 5, which were conducted under the same flow and sedimentary

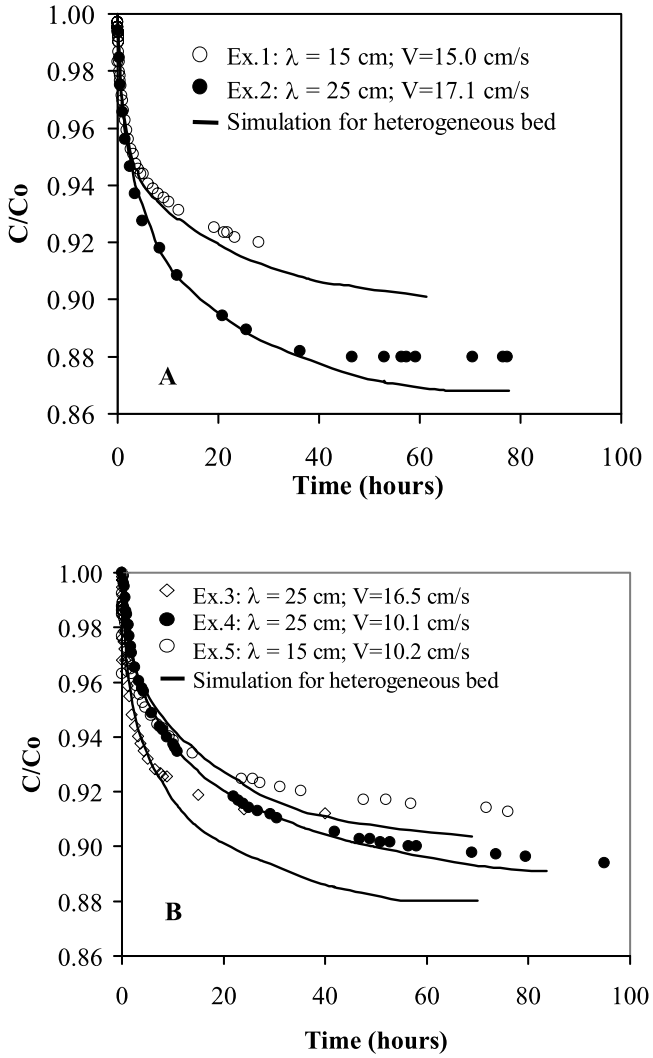

Figure 5. Comparisons of salt exchange results and model simulations with explicit representation of the bed structure: (a) Lower heterogeneity case (d_b = 22.5 cm) and (b) higher heterogeneity case (d_b = 15.5 cm).

conditions but with different bed form wavelengths. The shorter wavelength in experiment 5 produced faster initial exchange, but the exchange rate decreased relatively rapidly over time. On the other hand, the larger bed forms in experiment 4 produced comparatively slower initial exchange but the exchange rate decayed less rapidly than in experiment 5.

[41] Model simulations with assumption of a homogeneous bed and explicit representation of the sediment structure both did a reasonable job of predicting net solute exchange over the long timescales shown in Figures 4 and 5. The simulations with both bed structures overpredicted the exchange at later times. This discrepancy appeared to result from the fact that pore water velocities approached zero deep in the bed, producing numerical dispersion that resulted in significant errors in the calculation of net solute exchange at later stages of the simulation. Including the bed structure in the model improved simulation of exchange over all timescales. The model with explicit representation of the bed structure provided an excellent prediction of exchange for the first 30 hours of each experiment, as shown in Figure 6. Treating the beds as homogeneous still yielded reasonable predictions over this timescale, but with some underestimation of the net exchange rate.

[42] Assumption of a homogenous bed underestimated the observed exchange rate because heterogeneity produces an increase in the water flux across the stream-subsurface interface. Figure 7 shows the simulated interfacial water flux in experiment 5. For a homogeneous bed, the pattern of influx is identical for each bed form. Heterogeneity caused variable influx over the bed forms even though they had the same shape, and the average influx was 18% higher than that for the homogeneous bed. Similar trends were observed in simulations for all the experiments, with 15–20% higher influx found in model simulations with heterogeneous bed structure.

[43] The higher interfacial flux found with the heterogeneous beds occurs because of preferential pore water flow through higher-conductivity regions of the bed. Figure 8 shows the simulated hyporheic exchange streamlines for experiment 5. When the bed is homogeneous and the bed forms are regular, the same pore water flow field is found under all bed forms. Heterogeneity produces irregularity in the pore water flow. In addition, the bed has an effective anisotropy because of the 10:1 ratio of longitudinal and normal correlation length scales, and this produces steeper pore water head gradients in the longitudinal direction. Thus the simulated streamlines for the heterogeneous bed are flatter and more vertically compressed than those for the homogeneous bed. As a result, solutes move along shorter and faster preferential flow paths, and the overall penetration depth is reduced. A few preferential flow paths go deep into the bed, e.g., under bed forms 3, 4 and 8, but the head gradients, and thus the pore water velocities, drop off very rapidly with depth. Thus the simulations indicate little net vertical solute transport below approximately 8 cm depth. This explains why little additional net solute exchange was observed in experiments 1–5 after approximately 50 hours.

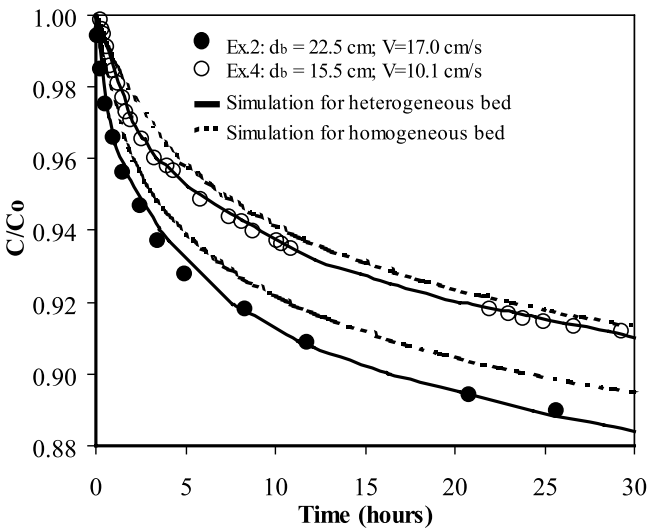

Figure 6. Comparison of model simulations with salt concentration data for first 30 hours of experiments 2 and 4. Similar results were found for the other experiments.

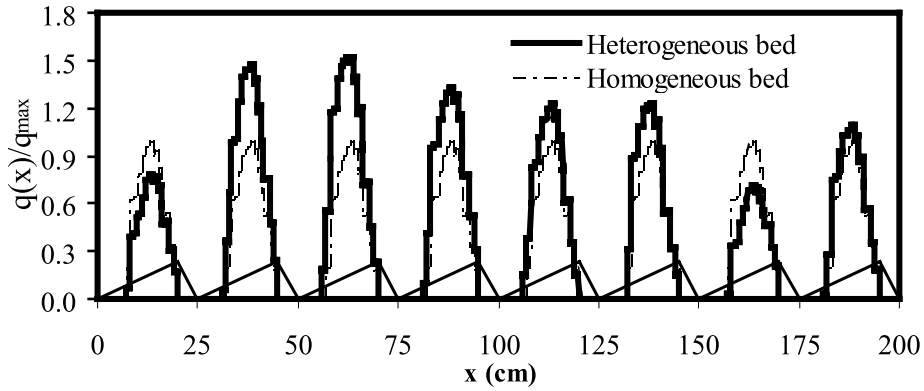

Figure 7. Simulated interfacial water flux through the eight bed forms in experiment 5. Flux is normalized to the maximum value for exchange with the homogeneous bed.

[44] The effect of heterogeneity on subsurface solute transport is further illustrated by the average residence time distributions shown in Figure 9. The average residence time function, $\bar{R}$, represents the fraction of a solute pulse at the bed surface that still remains in the bed after time t. The current rate of return solute flux from the bed to the stream is proportional to the slope of $\bar{R}$ (t). Figure 9 indicates that the return flux increases more quickly with a heterogeneous bed than with a homogeneous bed, i.e., solutes are initially transported through the hyporheic zone more quickly when the bed is heterogeneous. However, the slope of the residence time function for heterogeneous beds becomes much shallower than that for homogeneous beds at later times, indicating that the rate of solute release back to the stream water eventually becomes slower in the heterogeneous bed.

[45] These results emphasize the relationship between the bed structure, the pore water flow field, solute transport in pore waters, and net hyporheic exchange. Heterogeneity increased the rate of interfacial water flux and pore water velocities in the upper part of the bed while decreasing pore water velocities deeper in the bed. As a result, there was faster net solute mass transfer to the bed early in the experiments, but the exchange rate decreased more rapidly over time than it would have if the bed had been homogeneous. The overall effect of heterogeneity was thus that hyporheic exchange occurred at a greater rate but was more spatially limited.

[46] Two dye injection experiments were performed with the higher heterogeneity case ($\sigma^2_{\ln K} = 2.0$) and a bed form wavelength of 25 cm. Experiments 7 and 8 were performed with two different stream velocities, 14.0 and 10.1 cm/s, respectively. Figure 10 shows photographs of dye fronts beneath bed forms 2 and 3 taken at different times in experiment 8, along with the equivalent solute penetration fronts generated by the particle tracking model. The fronts reflect dye transport along hyporheic exchange streamlines. Initially, dye is transported through the upper homogeneous sediment layer containing the bed forms. During this period, the dye fronts appeared regular and were very similar to those observed previously with homogenous beds [*Elliott and Brooks*, 1997b]. As the dye moved into the underlying heterogeneous sediments, the dye was clearly observed to preferentially flow through coarser sediment blocks. These preferential flow paths altered the overall pattern of solute propagation through the bed. In the photograph for t = 1.15 hours, it can be seen that dye that had been rapidly transported along a horizontal preferential flow path under the bed form was beginning to move vertically upward into the low-pressure recirculation region downstream of the bed form crest. This caused the appearance of the wedge-shaped, dye-free regions that can be seen within each bed form. Clearly, hyporheic exchange occurred more rapidly via the underlying preferential flow path than directly through the bed form. At later times, dye propagated through the entire bed form and into deeper regions of the bed. The downward progression of dye fronts became increasingly slower with depth, and further dye penetration was difficult to discern after about 40 hours. These results are very consistent with the in-stream salt concentration data from experiments 1–6, which also indicated that heterogeneity enhanced solute flux to the bed early in the experiments but that the net mass transfer rate became extremely slow after 40 to 60 hours.

[47] The particle tracking model simulation based on the calculated pore water velocity field did a good job of predicting dye transport through the bed, including the locations of preferential flow paths. The success of the model in representing dye transport can particularly be seen in the accurate simulation of the irregular dye fronts near the downstream faces of the bed forms at t = 1.15 hours. The slight difference between the observed and simulated fronts probably occurred because of irregularities in the constructed bed, e.g., from blending of sands at the edges of blocks. The performance of the hyporheic exchange model is further illustrated in Figure 11, which compares the observed and simulated increase in the average dye penetration depth (M) with time. The average penetration depths in Figure 11 were obtained directly from the observed and simulated dye fronts shown in Figure 10. The model simulations closely matched the observed dye penetration depths in both experiments 7 and 8.

7. Discussion

[48] The experimental results and model simulations showed that heterogeneity had several distinct effects on hyporheic exchange. While observed net hyporheic exchange could be simulated reasonably well even with the assumption of a homogeneous bed, explicit representation of the bed structure was required for adequate prediction of interfacial fluxes and hyporheic exchange flow

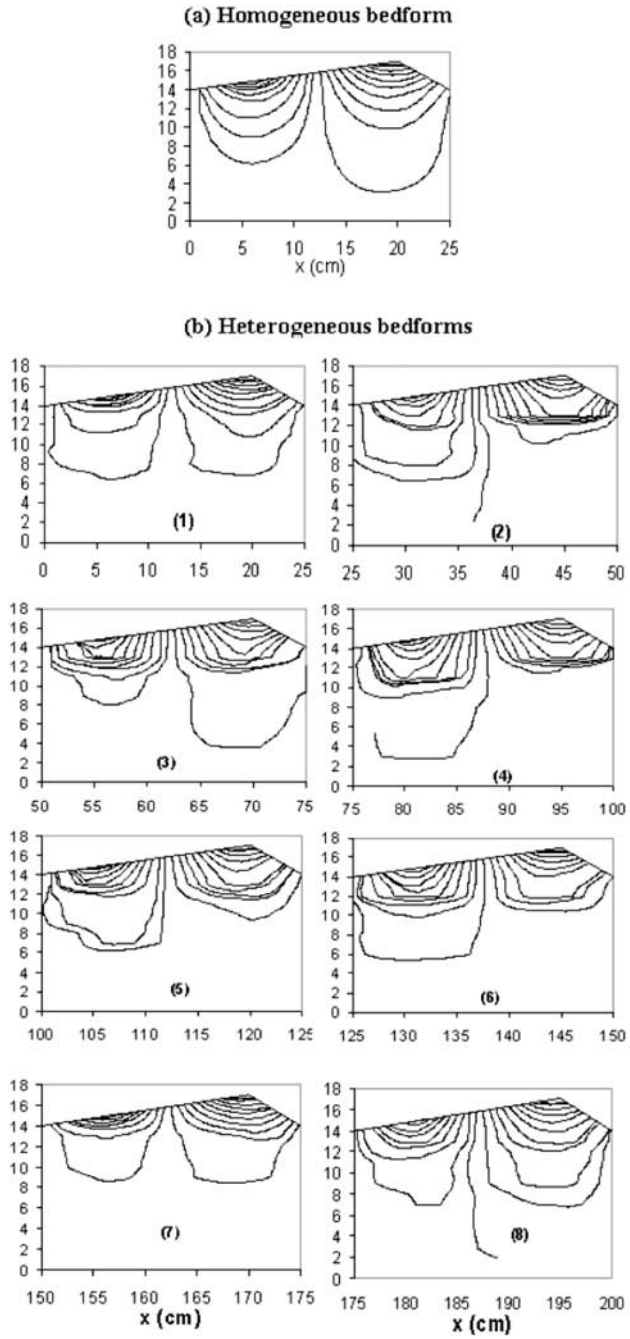

Figure 8. Simulated hyporheic flow paths in experiment 5 considering (a) an equivalent homogeneous bed and (b) the actual heterogeneous bed structure. These flow paths are equivalent to streamlines and were found by numerical particle tracking for a period of t = 70 hours.

paths. These results emphasize the distinction between hyporheic exchange flows and the net stream-subsurface exchange of solutes that results from those flows. A wide variety of models can be used to represent net hyporheic exchange [*Packman and Bencala*, 2000; *Wörman*, 2000]. However, only models based on explicit and detailed representation of stream-subsurface flow coupling processes can adequately predict the structure of hyporheic exchange flow paths and the resulting subsurface solute distributions. We will discuss here major findings on the structure of hyporheic exchange in heterogeneous streambeds and the implications for solute transport in natural streams.

7.1. Interfacial Flux

[49] Heterogeneity caused additional variability in hyporheic exchange flux across the stream-subsurface interface. Further, the average interfacial water flux was consistently greater for heterogeneous beds than for a homogeneous bed with the same mean permeability. This increase in the average stream-subsurface exchange flux occurs because of the nonlinear relationship between the heterogeneous hydraulic conductivity field and the pore water flow. For a homogeneous bed, solution of equations (1) and (2) yields Laplace's equation, a linear partial differential equation, for the pore water head distribution. For a homogeneous bed, equation (5) applies, and solution of this equation yields an average interfacial water flux that both depends on the heterogeneity of the permeability field and is greater than that for a homogeneous bed with the same mean permeability. This type of nonlinear transport behavior is well known from studies of groundwater flow [*Gelhar*, 1993].

[50] The finite element model provides a very useful tool for analysis of the spatial patterns of hyporheic exchange. This is particularly important for ecological applications because greater variability in physical transport conditions has been shown to increase benthic diversity and metabolism [*Boulton et al.*, 1998; *Bradley et al.*, 2002; *Sophocleous*, 2002]. In addition, analysis of the variability in interfacial water fluxes is critical for applications where solute fluxes must be averaged over a defined bed surface area. One example is the measurement of fluxes out of contaminated sediments, where an appropriate measurement scheme must be designed to obtain reliable estimates of net contaminant efflux. In this case uncertainty can arise from spatial variability in both contaminant distributions and pore water fluxes.

7.2. Hyporheic Flow Pathways

[51] Dye injection experiments clearly showed the existence of preferential hyporheic flow paths in the heterogeneous beds. The complex irregular features of the dye fronts

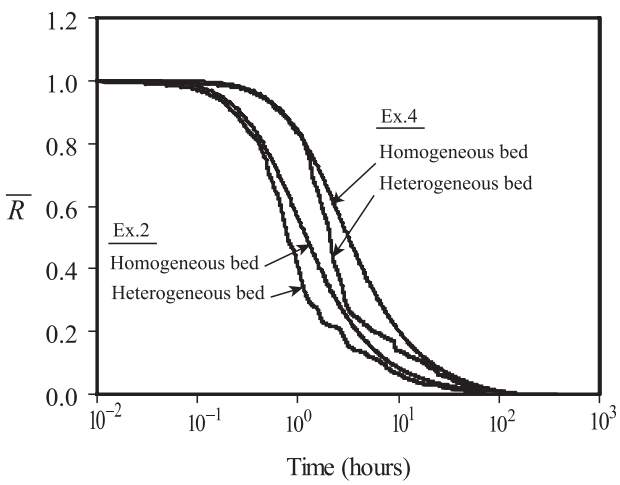

Figure 9. Average residence time distribution functions for heterogeneous beds and equivalent homogeneous beds.

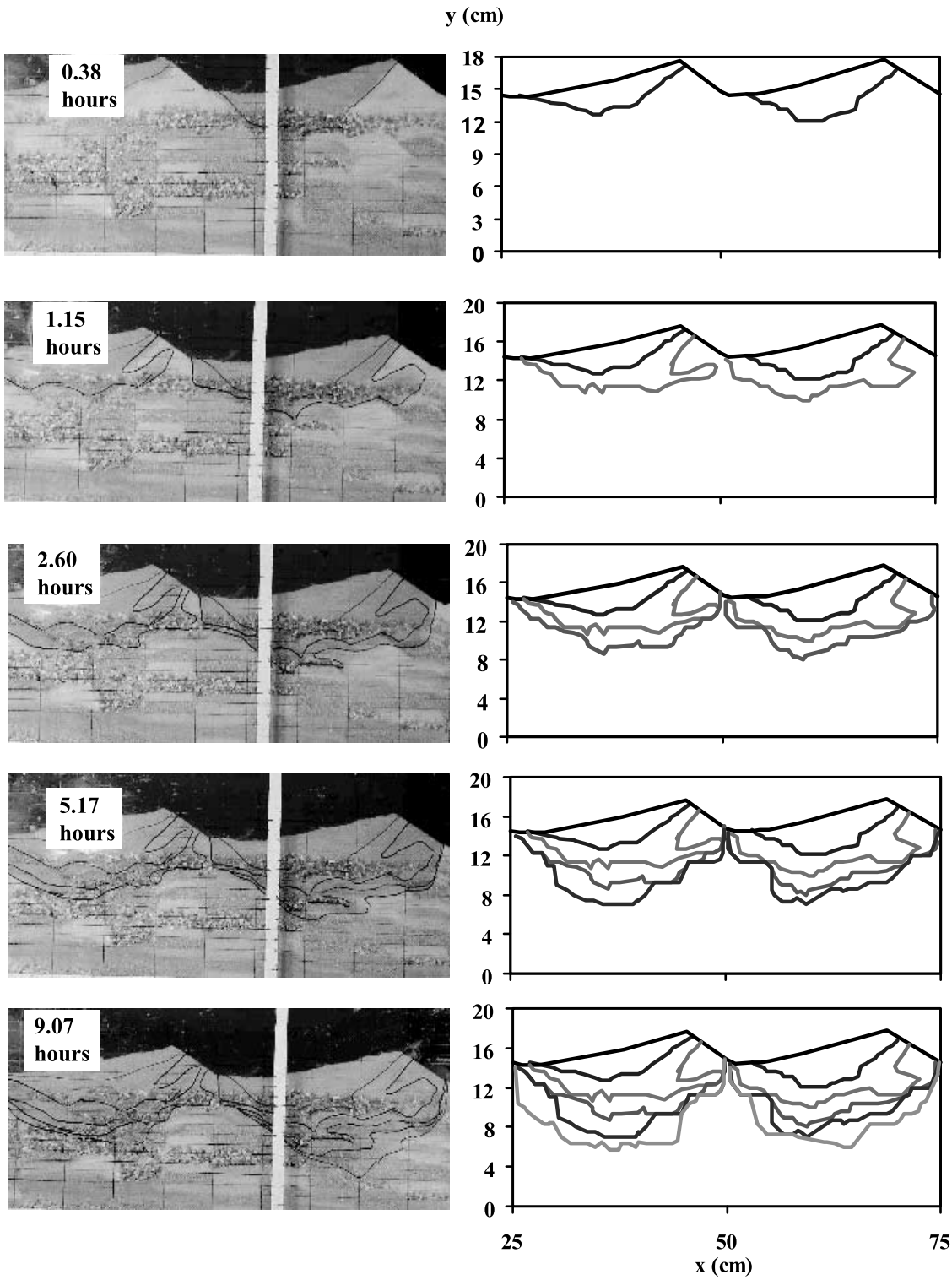

Figure 10. Observed dye fronts and the corresponding simulated solute penetration fronts for experiment 8. See color version of this figure at back of this issue.

observed here are very different from the regular smooth fronts that are found in homogeneous sand beds [*Elliott and Brooks*, 1997b]. The fact that the pore water flow model accurately simulated the observed dye fronts demonstrates the success of our explicit representation of sedimentary heterogeneity in a numerical model framework.

[52] Heterogeneity in pore water flows has considerable implications for the ecology and biogeochemistry of sediment beds. It is generally assumed that the hyporheic zone is well-oxygenated because of the penetration of stream water into this region [*Triska et al.*, 1989]. However, suboxic or anoxic zones can be found in low-transport

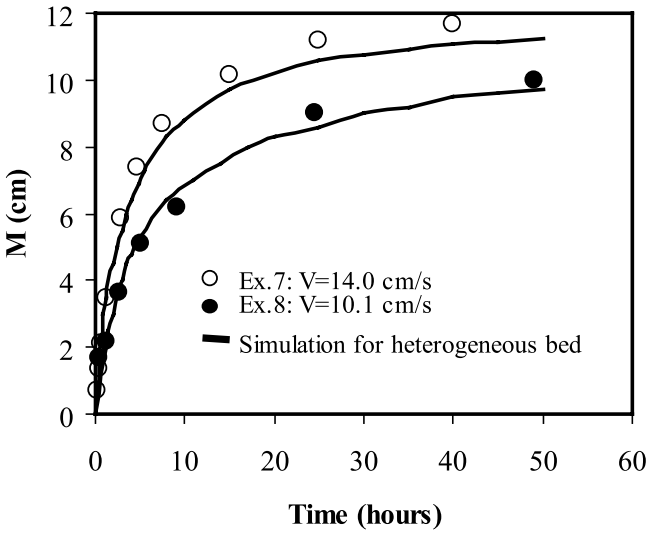

Figure 11. Comparison of observed and simulated average dye penetration depths in experiments 7 and 8.

microenvironments within the hyporheic zone [*Boulton et al.*, 1998]. The experimental results presented here clearly indicate that transport was very slow in low permeability regions of the streambed, and these regions are expected to have low oxygen levels in a bed with either reduced sediments or significant biological activity. The pore water redox patterns in a natural streambed generally result from complex feedbacks between physical transport, chemical reactions, and biological growth. While a variety of physical-chemical-biological feedbacks can alter the hyporheic transport environment, sediment structure clearly exerts considerable control on the pore water flow field and provides the fundamental physical template within which chemical and biological processes operate.

7.3. Penetration Depth and Solute Residence Time in the Hyporheic Zone

[53] The hyporheic exchange model predicted the observed dye penetration patterns in experiments with heterogeneous beds. Heterogeneity caused steeper pore water head gradients in the longitudinal direction so that the streamlines for the heterogeneous bed were more compressed than those found in homogeneous beds. Solutes moved along shorter and faster preferential hyporheic flow pathways, which produced more rapid net hyporheic exchange but shallower solute penetration into the subsurface. Thus heterogeneity produced a smaller hyporheic zone than would have occurred with homogeneous bed sediments.

[54] The decreased hyporheic penetration depth observed in our work is consistent with theory for groundwater flow in heterogeneous aquifers. *Gelhar and Axness* [1983] derived an effective hydraulic conductivity tensor using spectral perturbation analysis for an unbounded statistically anisotropic medium with horizontal isotropy ($l_x > l_y$) where the mean flow and solute transport are parallel to the bedding. For this case, the anisotropy of the effective hydraulic conductivity tensor ($\bar{K}_{xx}/\bar{K}_{yy}$) increases with increasing variance, $\sigma^2_{\ln K}$, and aspect ratio, l_x/l_y. Although the streambeds used here are bounded domains, the heterogeneous beds can still be considered as approximately equivalent homogeneous anisotropic systems. Following the analysis of Gelhar and Axness, the lower heterogeneity case had an effective anisotropy ratio $\bar{K}_{xx}/\bar{K}_{yy} \approx 2.5$, and the higher heterogeneity case had $\bar{K}_{xx}/\bar{K}_{yy} \approx 5$. This analysis clarifies the role of typical fluvial sedimentary structures in hyporheic exchange. The layered structure typically found in streambeds is expected to cause the induced pore water flow to be more horizontal and less vertical, and to thereby produce a more shallow hyporheic zone (less vertical penetration of solutes from the stream) with a higher mean hyporheic exchange rate.

[55] These results suggest that the size of hyporheic zones in natural streams will generally be controlled by the combined action of forcing by the overlying stream flow, the stream channel topography, and the structure of the underlying sediments. Streamflow over the channel topography (e.g., bed forms, meanders) produces head gradients that drive pore water flow. Larger head gradients, which can occur from higher stream velocity or other factors, will cause both more rapid flows and deeper solute penetration. Conversely, horizontally layered sediment structures will favor more rapid horizontal flow but will limit vertical solute penetration, producing a smaller hyporheic zone with a shorter mean hyporheic residence time.

7.4. Field Application

[56] While the results presented here show the effects of heterogeneity on hyporheic exchange in controlled laboratory experiments, natural streams show a very wide range of channel forms and sedimentary conditions. We recognize that the second-order stationary correlated random field model used here is an approximation that is not expected to adequately represent all fluvial sediment formations. More information on the fine-scale structural heterogeneity of stream channels and active fluvial environments will be necessary to adequately assess and predict the effects of sediment structure on hyporheic exchange in natural systems. Nonetheless, we expect that the basic trends observed here will generally hold in fluvial systems. Further, the dual FEM and particle-tracking modeling approach presented here can be applied to analyze three-dimensional hyporheic exchange flow paths and solute transport in natural systems, provided that the requisite model input parameters are measured in sufficient detail. The information gained from this study can thus be further refined and applied to different streams as more data becomes available on the fine-scale structure of streambed sediments.

8. Concluding Remarks

[57] We carried out salt and dye injection experiments in a recirculating flume packed as a correlated random heterogeneous bed designed with a stochastic approach. The experimental results were successfully simulated by a numerical model that predicts the pore water flow field and resulting hyporheic exchange based on fundamental analysis of stream-subsurface flow coupling and an explicit and detailed representation of the streambed structure. To the best of our knowledge, this work represents the first experimental study of hyporheic exchange with a well-defined heterogeneous porous medium and the first simulation of hyporheic exchange with explicit analysis of the effects of the underlying heterogeneous sediment structure.

[58] Streambed heterogeneity caused additional variability in flux across the stream-subsurface interface and the development of preferential subsurface flow paths. Heterogeneity also produced greater average interfacial water flux, less vertical solute penetration, and a shorter mean hyporheic residence time. These effects should generally be seen in natural streams. The numerical exchange model did a very good job of simulating the observed pore water flow paths, mean solute penetration, and net stream-subsurface exchange over a reasonable timescale (to around 30 hours). While the model presented here can be applied in the field, the structure of fluvial sediments is not known in sufficient detail to allow prediction of these effects in natural streams. Future studies should focus on obtaining more detailed information on the permeability structure of streambed sediments in order to specifically examine relationships between fluvial sediment dynamics, streambed heterogeneity, and hyporheic exchange.

Notation

- C tracer concentration in the stream.
- C_0 initial tracer concentration in the stream.
- C^* dimensionless tracer concentration, $C^* = C/C_0$.
- d average stream depth.
- d_b streambed depth.
- d' effective water column depth, the total volume of stream water per unit bed area.
- d_x Grain diameter for which x% of the sediment is finer.
- g acceleration due to gravity.
- h_m half-amplitude of the sinusoidal pressure distribution at the bed surface.
- h head.
- H average bed form height (trough to crest).
- k bed form wave number, $k = 2\pi/\lambda$.
- K hydraulic conductivity of bed sediment.
- K_{xx} hydraulic conductivity in the principal x direction.
- $\overline{K}_{xx}$ effective hydraulic conductivity in the principal x direction.
- K_{yy} hydraulic conductivity in the principal y direction.
- $\overline{K}_{yy}$ effective hydraulic conductivity in the principal y direction.
- l_x correlation length scale of hydraulic conductivity in the horizontal direction.
- l_y correlation length scale of hydraulic conductivity in the vertical direction.
- L length of the sediment bed in the downstream direction.
- $\ln K$ natural logarithm of hydraulic conductivity.
- $\overline{\ln K}$ mean value of lnK.
- M average depth of solute penetration into the streambed.
- $\overline{n}$ unit vector normal to the bed surface pointing outward.
- $N(s)$ total number of data pairs for analysis of correlation of the hydraulic conductivity field.
- q local pore water flux through the bed surface.
- $\overline{q}$ average pore water flux through the bed surface.
- R residence time distribution function.
- $\overline{R}$ average residence time distribution function.
- s separation distance.
- t time.
- dt incremental time step.
- u horizontal Darcy velocity component.
- u_m maximum Darcy velocity, $u_m = kKh_m$.
- $\overline{v}$ Darcy velocity vector, $\overline{v} = (u, v)$.
- v vertical Darcy velocity component.
- V average stream velocity over the cross section of the stream.
- x longitudinal coordinate along the streambed (parallel to the mean bed surface).
- X location of sample hydraulic conductivity in variogram analysis.
- y normal coordinate perpendicular to the mean bed surface.
- λ bed form wavelength.
- θ porosity of the sediments.
- γ variogram or semivariogram.
- τ time elapsed since solute entered the bed.
- $\sigma^2_{\ln K}$ variance of lnK data.

[59] **Acknowledgment.** The authors gratefully acknowledge financial support for this research through NSF CAREER award BES-0196368 and additional support provided by the Pepper Foundation for undergraduate research at Northwestern University.

References

Ababou, R., D. B. McLaughlin, L. W. Gelhar, and A. F. B. Tompson (1989), Numerical simulation of three-dimensional saturated flow in randomly heterogeneous porous media, *Transp. Porous Media*, *4*(6), 549–566.

Bakr, A. A., L. W. Gelhar, A. L. Gutjahr, and J. R. MacMillan (1978), Stochastic analysis of spatial variability in subsurface flows: 1. Comparison of one- and three-dimensional flows, *Water Resour. Res.*, *14*(2), 263–271.

Baxter, C. V., and F. R. Hauer (2000), Geomorphology, hyporheic exchange, and selection of spawning habitat by bull trout (*Salvelinus confluentus*), *Can. J. Fish. Aquat. Sci.*, *57*, 1470–1481.

Bencala, K. E., and R. A. Walters (1983), Simulation of solute transport in a mountain pool-and-riffle stream: A transient storage model, *Water Resour. Res.*, *19*(3), 718–724.

Boulton, A. J., S. Findlay, P. Marmonier, E. H. Stanley, and M. Valett (1998), The functional significance of the hyporheic zone in streams and rivers, *Annu. Rev. Ecol. Syst.*, *29*, 59–81.

Bradley, J. C., M. A. Palmer, C. M. Swan, and S. Brooks (2002), The influence of substrate heterogeneity on biofilm metabolism in a stream ecosystem, *Ecology*, *83*(2), 412–422.

Bridge, J. S. (1993), Description and interpretation of fluvial deposits—A critical perspective, *Sedimentology*, *40*(4), 801–810.

Bridge, J. S., J. Alexander, R. Collier, R. L. Gawthorpe, and J. Jarvis (1995), Ground-penetrating radar and coring used to study the large-scale structure of point-bar deposits in 3 dimensions, *Sedimentology*, *42*(6), 839–852.

Brunke, M., and T. Gonser (1997), The ecological significance of exchange processes between rivers and groundwater, *Freshwater Biol.*, *37*(1), 1–33.

Buffington, J. M., and D. R. Montgomery (1999a), Effects of hydraulic roughness on surface textures of gravel-bed rivers, *Water Resour. Res.*, *35*(11), 3507–3521.

Buffington, J. M., and D. R. Montgomery (1999b), Effects of sediment supply on surface textures of gravel-bed rivers, *Water Resour. Res.*, *35*(11), 3523–3530.

Cerling, T. E., S. J. Morrison, R. W. Sobocinski, and I. L. Larsen (1990), Sediment-water interaction in a small stream: Adsorption of ^{137}Cs by bed load sediments, *Water Resour. Res.*, *26*(6), 1165–1176.

Chao, H. C., H. Rajaram, and T. Illangasekare (2000), Intermediate-scale experiments and numerical simulations of transport under radial flow in a two-dimensional heterogeneous porous medium, *Water Resour. Res.*, *36*(10), 2869–2884.

Church, M., M. A. Hassan, and J. F. Wolcott (1998), Stabilizing self-organized structures in gravel-bed stream channels: Field and experimental observations, *Water Resour. Res.*, *34*(11), 3169–3179.

Colbeck, S. C. (1989), Air movement in snow due to wind pumping, *J. Glaciol.*, *35*(120), 209–213.

Colbeck, S. C. (1997), Model of wind pumping for layered snow, *J. Glaciol.*, *43*(143), 60–65.

Elliott, A. H., and N. H. Brooks (1997a), Transfer of nonsorbing solutes to a streambed with bedforms: Theory, *Water Resour. Res.*, *33*(1), 123–136.

Elliott, A. H., and N. H. Brooks (1997b), Transfer of nonsorbing solutes to a streambed with bedforms: Laboratory experiments, *Water Resour. Res.*, *33*(1), 137–151.

Gelhar, L. W. (1993), *Stochastic Subsurface Hydrology*, Prentice-Hall, Old Tappan, N. J.

Gelhar, L. W., and C. L. Axness (1983), Three dimensional stochastic analysis of macrodispersion in aquifers, *Water Resour. Res.*, *19*(1), 161–180.

Haggerty, R., S. M. Wondzell, and M. A. Johnson (2002), Power law residence time distribution in the hyporheic zone of a 2nd order mountain stream, *Geophys. Res. Lett.*, *29*(13), 1640, doi:10.1029/2002GL014743.

Harvey, J. W., and K. E. Bencala (1993), The effect of streambed topography on surface-subsurface water exchange in mountain catchments, *Water Resour. Res.*, *29*(1), 89–98.

Hess, K. M., S. H. Wolf, and M. A. Celia (1992), Large-scale natural gradient tracer test in sand and gravel, Cape Cod, Massachusetts: 3. Hydraulic conductivity variability and calculated macrodispersivities, *Water Resour. Res.*, *28*(8), 2011–2028.

Huettel, M., W. Ziebis, and S. Forster (1996), Flow-induced uptake of particulate matter in permeable sediments, *Limnol. Oceanogr.*, *41*(2), 309–322.

Huggenberger, P., E. Hoehn, R. Beschta, and W. Woessner (1998), Abiotic aspects of channels and floodplains in riparian ecology, *Freshwater Biol.*, *40*, 407–425.

Hutchinson, P. A., and I. T. Webster (1998), Solute uptake in aquatic sediments due to current-obstacle interactions, *J. Environ. Eng.*, *124*(5), 419–426.

Jones, J. B., and P. J. Mulholland (Eds.) (2000), *Streams and Ground Waters*, Academic, San Diego, Calif.

Journel, A. G., and C. J. Huijbregts (1978), *Mining Geostatistics*, Academic, San Diego, Calif.

Leopold, L. B., M. G. Wolman, and J. P. Miller (1964), *Fluvial Processes in Geomorphology*, W.H. Freeman, New York.

Lisle, T. E., J. M. Nelson, J. Pitlick, M. A. Madej, and B. L. Barkett (2000), Variability of bed mobility in natural, gravel-bed channels and adjustments to sediment load at local and reach scales, *Water Resour. Res.*, *36*(12), 3743–3755.

Medina, M. A., R. L. Doneker, N. Grosso, D. M. Johns, W. Lung, M. F. N. Mohsen, A. I. Packman, and P. J. Roberts (2004), Surface water-ground water interactions and modeling applications, in *Contaminated Ground Water and Sediment: Modeling for Management and Remediation*, edited by C. C. Chien et al., pp. 1–62, CRC Press, Boca Raton, Fla.

Naegeli, M. W., P. Huggenberger, and L. Uehlinger (1996), Ground penetrating radar for assessing sediment structures in the hyporheic zone of a prealpine river, *J. N. Am. Benth. Soc.*, *15*(3), 353–366.

Neuman, S. P., A. L. Winter, and C. M. Newman (1987), Stochastic theory of field scale dispersion in anisotropic porous media, *Water Resour. Res.*, *23*(3), 453–466.

Packman, A. I., and K. E. Bencala (2000), Modeling methods in the study of surface-subsurface hydrologic interactions, in *Streams and Ground Waters*, edited by J. B. Jones and P. J. Mulholland, pp. 45–80, Academic, San Diego, Calif.

Packman, A. I., and M. Salehin (2003), Relative roles of stream flow and sedimentary conditions in controlling hyporheic exchange, *Hydrobiologia*, *494*, 291–297.

Packman, A. I., N. H. Brooks, and J. J. Morgan (2000a), A physicochemical model for colloid exchange between a stream and a sand streambed with bed forms, *Water Resour. Res.*, *36*(8), 2351–2361.

Packman, A. I., N. H. Brooks, and J. J. Morgan (2000b), Kaolinite exchange between a stream and streambed: Laboratory experiments and validation of a colloid transport model, *Water Resour. Res.*, *36*(8), 2363–2372.

Parker, G., and P. C. Klingeman (1982), On why gravel bed streams are paved, *Water Resour. Res.*, *18*(5), 1409–1423.

Powell, D. M. (1998), Patterns and processes of sediment sorting in gravel-bed rivers, *Prog. Phys. Geogr.*, *22*(1), 1–32.

Rehfeldt, K. R., J. M. Boggs, and L. W. Gelhar (1992), Field study of dispersion in a heterogeneous aquifer: 3. Geostatistical analysis of hydraulic conductivity, *Water Resour. Res.*, *28*(12), 3309–3324.

Ren, J., and A. I. Packman (2002), Effects of particle size and background water composition on stream-subsurface exchange of colloids, *J. Environ. Eng.*, *128*(7), 624–634.

Robert, A. (1993), Bed configuration and microscale processes in a alluvial channels, *Prog. Phys. Geogr.*, *17*(2), 123–136.

Salehin, M., A. I. Packman, and A. Wörman (2003), Comparison of hyporheic exchange in vegetated and unvegetated reaches of a small agricultural stream in Sweden: Seasonal variation and anthropogenic manipulation, *Adv. Water Resour.*, *26*(9), 951–964.

Savant, S. A., D. D. Reible, and L. J. Thibodeax (1987), Convective transport within stable river sediments, *Water Resour. Res.*, *23*(9), 1763–1768.

Sophocleous, M. (2002), Interactions between groundwater and surface water: The state of the science, *Hydrogeol. J.*, *10*, 52–67.

Stanford, J. A., and T. Gonser (Eds.) (1998), Rivers in the landscape: riparian and groundwater ecology, *Freshwater Biology*, *40*(3), 185 pp.

Thibodeax, L. J., and J. D. Boyle (1987), Bedform-generated convective transport in bottom sediment, *Nature*, *325*(22), 341–343.

Tompson, A. F. B., and L. W. Gelhar (1990), Numerical simulation of solute transport in three-dimensional, randomly heterogeneous porous media, *Water Resour. Res.*, *26*(10), 2541–2562.

Tompson, A. F. B., R. Ababou, and L. W. Gelhar (1989), Implementation of the three-dimensional turning bands random field generator, *Water Resour. Res.*, *25*(10), 2227–2243.

Triska, F. J., V. C. Kennedy, R. J. Avanzino, G. W. Zellweger, and K. E. Bencala (1989), Retention and transport of nutrients in a third-order stream in northwestern California: Hyporheic process, *Ecology*, *70*, 1893–1905.

Vandenberghe, J., and R. A. van Overmeeren (1999), Ground penetrating radar images of selected fluvial deposits in the Netherlands, *Sediment. Geol.*, *128*(3–4), 245–270.

Welty, C., and M. M. Elsner (1997), Constructing correlated random fields in the laboratory for observations of fluid flow and mass transport, *J. Hydrol.*, *202*(1/4), 67–82.

Whiting, P. J., and J. G. King (2003), Surface particle sizes on armoured gravel streambeds: Effects of supply and hydraulics, *Earth Surf. Processes Landforms*, *28*(13), 1459–1471.

Wondzell, S. M., and F. J. Swanson (1996), Seasonal and storm dynamics of the hyporheic zone of a 4th order mountain stream, 1, Hydrologic processes, *J. N. Am. Benthol. Soc.*, *15*(1), 3–19.

Wörman, A. (1998), Analytical solution and timescale for transport of reacting solutes in rivers and streams, *Water Resour. Res.*, *34*(10), 2703–2716.

Wörman, A. (2000), Comparison of models for transient storage in small streams, *Water Resour. Res.*, *36*(2), 455–468.

Wörman, A., A. I. Packman, H. Johansson, and K. Jonsson (2002), Effect of flow-induced exchange in hyporheic zones on longitudinal transport of solutes in streams and rivers, *Water Resour. Res.*, *38*(1), 1000, doi:10.1029/2000WR000211.

Wroblicky, G. J., M. E. Campana, H. M. Valett, and C. N. Dahm (1998), Seasonal variation in surface-subsurface water exchange and lateral hyporheic area of two stream-aquifer systems, *Water Resour. Res.*, *34*(3), 317–328.

Young, P. C., and S. G. Wallis (1993), Solute transport and dispersion in channels, in *Channel Network Hydrology*, edited by K. J. Beven and M. J. Kirby, pp. 129–174, John Wiley, Hoboken, N. J.

A. I. Packman and M. Paradis, Department of Civil and Environmental Engineering, Northwestern University, 2145 Sheridan Road, Evanston, IL 60208-3109, USA.

M. Salehin, Institute of Water and Flood Management, Bangladesh University of Engineering and Technology, Dhaka-1000, Bangladesh. (mashfiqussalehin@iwfm.buet.ac.bd)

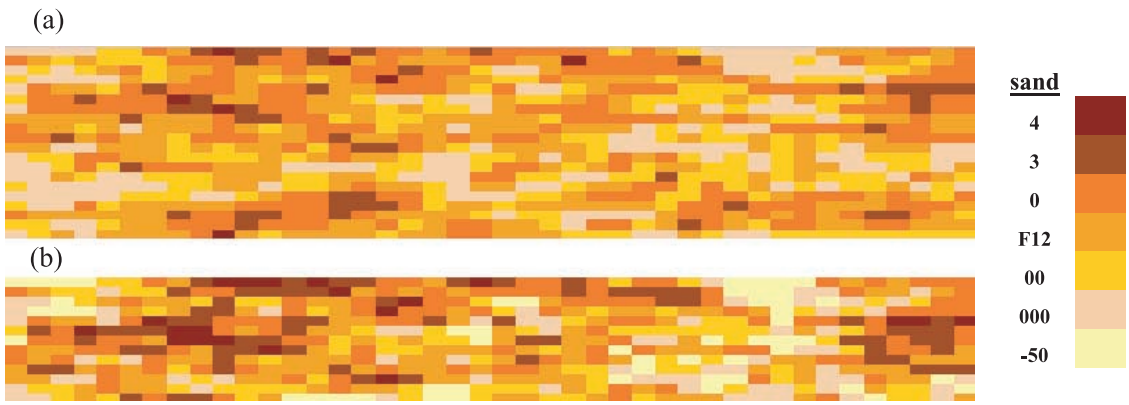

Figure 1. Two-dimensional heterogeneous packing designs based on synthetic generation of correlated random hydraulic conductivity fields: (a) Lower heterogeneity case and (b) higher heterogeneity case. Each block is 5 cm × 1 cm.

Figure 3. Lower heterogeneity bed in the recirculating flume. The grid on the channel sidewall is color-coded to indicate the sand type in each block.

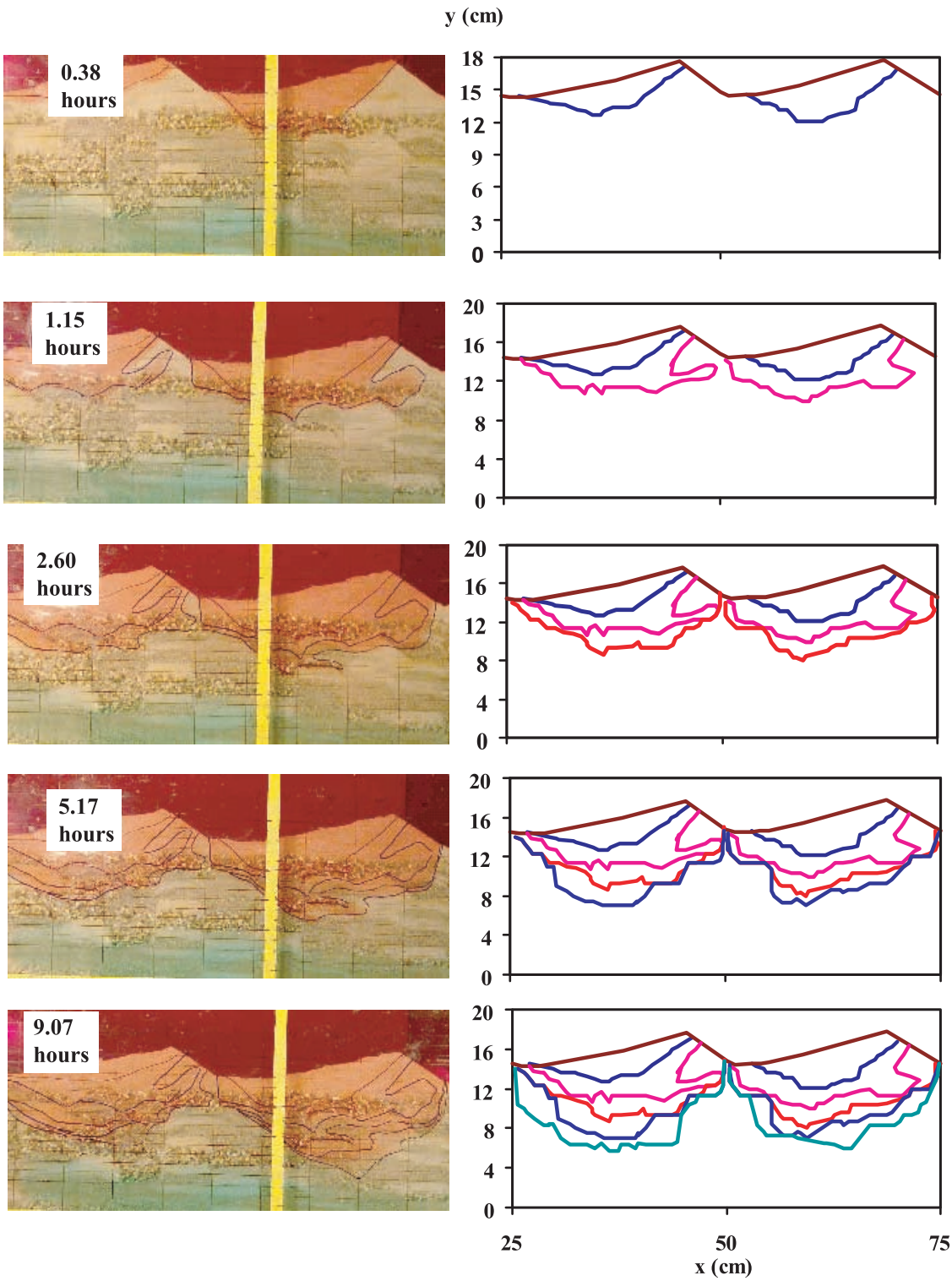

Figure 10. Observed dye fronts and the corresponding simulated solute penetration fronts for experiment 8.